

铝合金点焊位移信号时频域分析与质量判定

潘存海¹, 杜素梅¹, 宋永伦²

(1. 天津科技大学 机械工程学院, 天津 300222;
2. 北京工业大学 机电工程学院, 北京 100085)



潘存海

摘 要: 采用分布式多传感器同步采集系统实现了铝合金点焊质量实时监测。通过位移信号时频域分析发现, 飞溅焊点位移信号在 40~80 Hz 范围内, Butterworth 带通滤波极差达 0.5 mm 左右; 未熔合或未完全熔合焊点的位移信号极差比另外两类焊点低 1.0 mm 左右。利用上述明显特征信息可以实现点焊质量人工判定。由于位移信号信噪比高, 特征提取算法简洁, 进一步可实现机器在线判读。同时, 利用统计分析, 样本 197 个, 在合格区内焊点正确判断率达 97.6%。

关键词: 电阻点焊; 铝合金; 位移信号; 时频域分析; 质量判定
中图分类号: TG409 文献标识码: A 文章编号: 0253-360X(2007)07-033-04

0 序 言

铝合金具有优异的导电性能和良好的导热性能, 通常采用大电流、短时间的硬参数进行点焊。在实际生产中, 由于受工件表面状态、电极磨损、装配间隙和机械结构等诸多因素的影响, 即使按照相同焊接参数组织生产, 仍然有可能出现质量波动。铝合金点焊过程控制精度高, 难度大, 容易产生飞溅、未熔合和未完全熔合等缺陷。目前, 点焊仍缺乏可靠、实用的无损检测技术和方法, 因此利用现代传感技术实现点焊质量全面监测已经成为该领域的研究热点^[1]。

许多研究者已经注意到点焊过程比较复杂, 采用多传感器监测点焊过程十分必要。其中, 电极位移和电极压力信息引人关注^[1-3]。但是, 为了保证在线质量监测系统可靠实用, 一方面, 点焊传感器数量应尽量减少, 数据预处理、数据压缩与特征提取的算法简洁, 特征信息与质量对应关系简单明确; 另一方面, 在使用过程中, 数据样本要具备不断完善和扩充的能力。

作者采用多传感器同步采集系统实现了铝合金点焊质量的实时监测。电极位移信号信噪比高, 特征信息明显, 重复性好, 能够反映出点焊合格、飞溅、

未熔合和未完全熔合等质量信息。采用小波变换和统计分析方法提取特征信息, 算法简洁、实用。通过基于 LabView 的 Butterworth 带通滤波证实可以采用硬件直接提取点焊飞溅信息, 为今后硬件设计提供了试验和理论依据。

1 小波变换理论基础

$f(t)$ 线性分解 $f(t) = \sum_k \alpha_k \varphi_k(t)$ 结果唯一的条件为, 当 $k \neq l$ 时, 内积为零, 如式(1)所示, 即 $\varphi_k(t)$ 为正交基。其中, $f(t)$ 为待分析的信号函数; $\varphi_k(t)$ 为选用的小波函数; α_k 为系数, α_k 的确定方法如式(2)所示。

$$[\varphi_k(t), \varphi_l(t)] = \int \varphi_k(t) \overline{\varphi_l(t)} dt = 0. \quad (1)$$

$$\alpha_k = [f(t), \varphi_k(t)] = \int f(t) \overline{\varphi_k(t)} dt. \quad (2)$$

上述过程互逆。

双参数系有类似结果, 其中, $f(t)$ 为待分析的信号函数; $\varphi_{j,k}(t)$ 为选用的小波函数; $\alpha_{j,k}$ 为系数。

$$f(t) = \sum_k \sum_j \alpha_{j,k} \varphi_{j,k}(t), \quad (3)$$

$$\alpha_{j,k} = [f(t), \varphi_{j,k}(t)] = \int f(t) \overline{\varphi_{j,k}(t)} dt.$$

实际上这就是小波变换的本质。

基于 $\varphi_{a,b}(t)$ 小波函数的 $f(t)$ 连续小波变换 (continuous wavelet transform, CWT) 最常使用的小

收稿日期: 2006-10-08
基金项目: 天津市自然科学基金资助项目(05YFJMJC02600); 天津科技大学人才引进项目(20050404)

波变换表达式 $(CWT_{\varphi} f)(a, b)^{[4]}$ 为

$$(CWT_{\varphi} f)(a, b) = [f(t), \varphi_{a,b}(t)] = |a|^{-1/2} \int_{-\infty}^{+\infty} f(t) \frac{\varphi(t-b)}{a} dt, \quad (4)$$

$a \neq 0$, 且 $a \in R; b \in R$.

式中: $\varphi_{a,b}(t)$ 称为小波函数 (wavelet function), 该函数是由时间尺度 a 和时间平移 b 两个参量确定的时间函数。一旦 a 和 b 确定, 就相当于确定了一个短时傅里叶变换 (STFT), 一系列的 a 和 b 对应一组短时傅里叶变换的汇集。小波变换可以根据需要同时分析时域和频域信息。

多分辨率分析 (MRA) 不仅为正交小波基构造提供了一种简单的方法, 而且为正交小波变换的快速算法提供了理论依据^[5]。小波分解实际上是将测试信号中不同频率的信息抽取出来, 并投影到统一参照系的时间轴上进行比较分析。根据信号的特点选择小波种类和分解层数, 即可对信号同时进行时域和频域分析。文中选择 DB3 level 7 对点焊位移信号进行小波分解, 并对小波细节分量做统计分析。

2 试验方法与设备

铝合金点焊设备为 DJ-1000 型直流点焊机。铝合金为 LF6 和 LD10CS 板材。其中, LF6 板厚为 2.5 mm, LD10CS 板厚为 5.5 mm, 两种板材组合成搭接接头, 焊前经过严格机械打磨和化学清洗。

基于 RS485 分布式单片机同步数据采集系统采用电流、电压、电极位移和电极压力四种传感器, 同步采集 5 s, 采样频率 10 kHz, 12 位精度。工作原理如图 1 所示, 利用 LabView 图形化语言编制了相关数据处理软件, 该软件具备数据规格化、数据滤波、数据统计、特征提取与质量评定等功能。

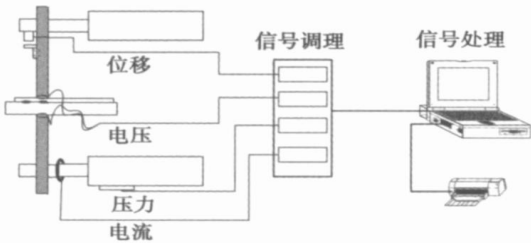


图 1 点焊监测系统

Fig. 1 Monitoring system diagrammatic drawing of resistance spot welding

自行设计制作了大电流传感器, 内径为 110 mm, 匝数为 1 400 匝, 横断面呈矩形扁带^[1]。位移传感器

温度漂移每度不超过 0.025%, 频率响应为 0~10 kHz, 线性范围 3~13 mm, 电压信号输出 0~10 V。压力传感器频率响应 10 kHz, 在 5~50 °C 温度范围内, 温度漂移每度不超过 0.07%。利用分别固定在点焊机上、下电极的双绞线测量电极电压信号。

3 试验结果与讨论

3.1 点焊位移信号时频域分析结果与讨论

图 2 所示为三种典型点焊位移信号采用 DB3 号小波分解结果, a_7 为位移 D 的逼近信号, d_7 , d_6 , d_5 和 d_4 分别表示各层细节信号, 四层以下的细节信号主要是高频信息, 没有明显的特征 (省略)。

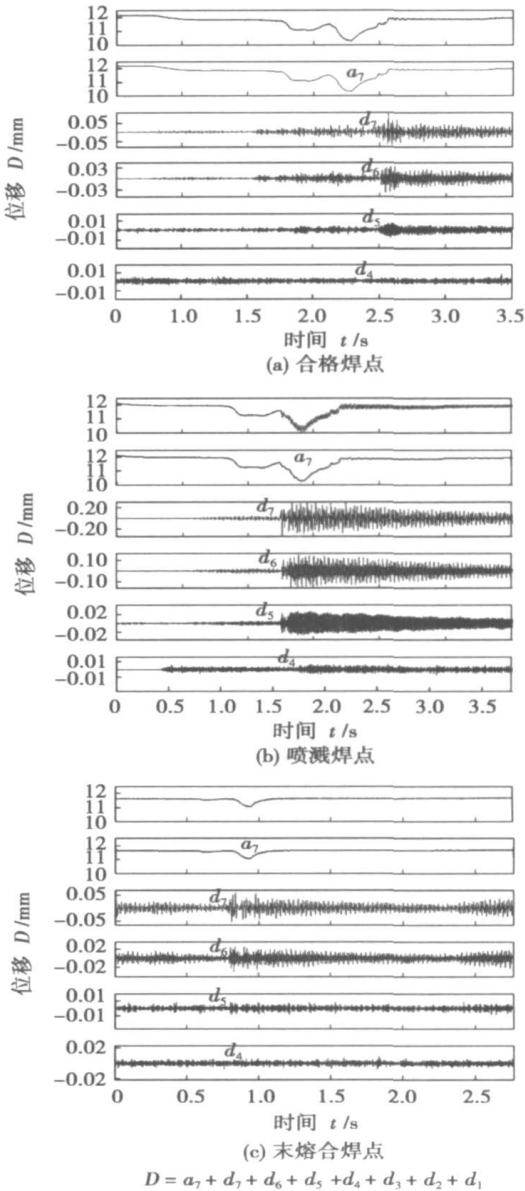


图 2 点焊位移信号小波分析

Fig. 2 Displacement signal wavelet analysis of RSW

通过对比发现,图 2b 点焊内喷溅位移信号的 d_7 细节分量极差达到 0.5 mm 左右,明显大于其它两类焊点;而图 2c 原始位移信号 D 的极差明显小于其它两类焊点,相差达 1.0 mm 左右,点焊质量特征信息明显。利用点焊电极位移信号可以评定焊点质量。同时,根据采样频率(5 000 Hz)和小波分解各层频率结构关系可以确定 a_7 , d_7 , d_6 , d_5 和 d_4 对应的频率范围分别为 $[0, 39 \text{ Hz}]$, $[39 \text{ Hz}, 78 \text{ Hz}]$, $[78 \text{ Hz}, 156 \text{ Hz}]$ 和 $[156 \text{ Hz}, 312 \text{ Hz}]^{[1]}$ 。

通过小波分析发现,点焊位移特定频率信息与喷溅缺陷存在对应关系。图 3 进一步利用 LabView 实现了位移信号 Butterworth 中频带通滤波。

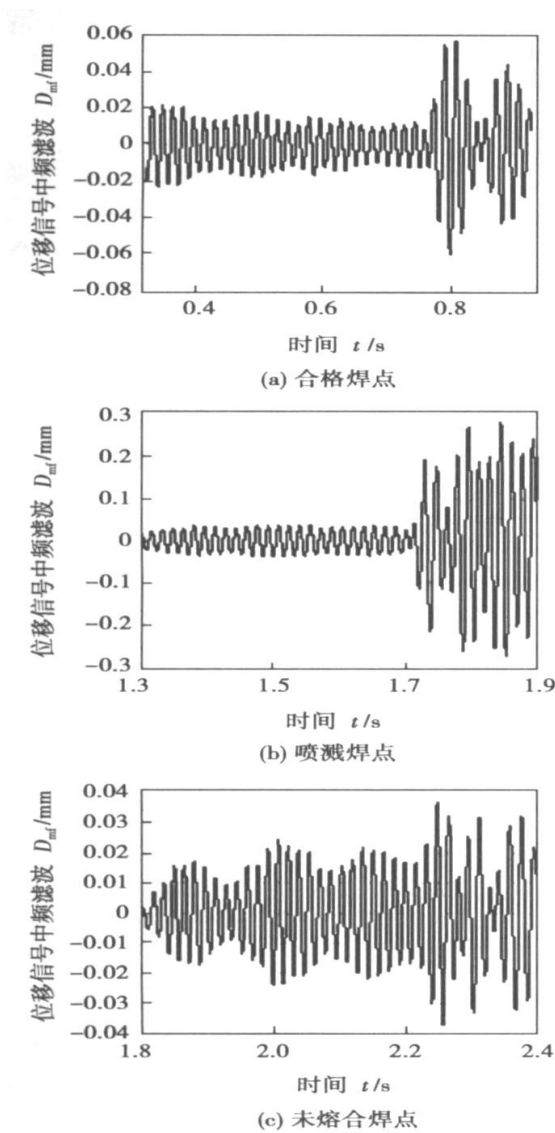


图 3 点焊位移信号中频滤波

Fig. 3 Displacement signal MF filtering of RSW

图 3a, b, c 分别为图 2a, b, c 的局部中频带通滤波,频率范围为 40 ~ 80 Hz。图 3b 喷溅焊点中频带

通滤波极差为 0.5 mm 左右,与小波分析一致,因此可以通过硬件提取喷溅特征。

3.2 点焊位移信号统计分析

焊点质量分三类,合格焊点、喷溅焊点和未熔合或未完全熔合焊点。通过解剖观察焊点是否喷溅,按照国内企业标准 QB2205 — 95 确定焊点直径是否合格。

图 4 所示为 DB3 小波 7 水平细节分量与焊点直径对应关系的统计分布。统计样本共 197 个焊点,点焊工艺参数 3 种,分别对应 B01, B04 和 B05,为了表达更清晰,每种工艺参数只区分合格和不合格焊点。其中, B01 焊点样本 117 个; B04 焊点样本 33 个,喷溅倾向比较大; B05 焊点样本 47 个。由此可以看出,相同点焊工艺参数,焊点质量并不能保证完全一致,因此全面监测点焊过程十分必要。

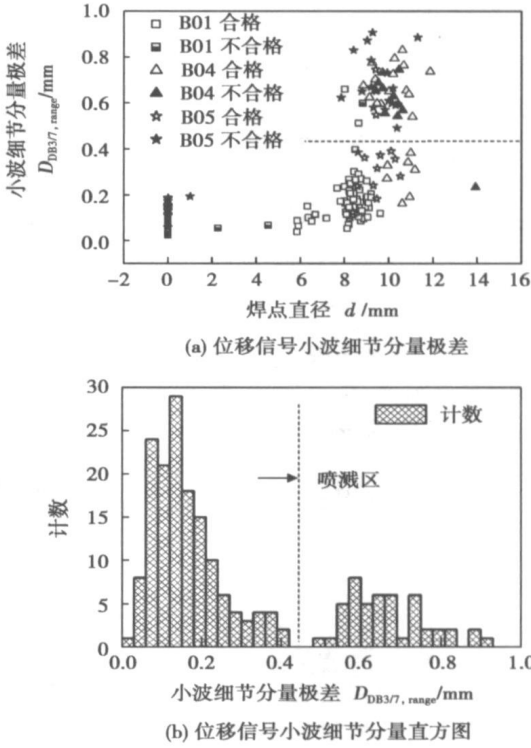


图 4 位移信号小波细节分量极差与焊点直径的关系
Fig. 4 Relationship between displacement signal $D_{DB3/7}$ range and welding spot diameter

从图 4a 可以看出,喷溅焊点主要分布在上半部分,换言之,喷溅焊点位移信号小波细节分量的极差 $D_{DB3/7, range}$ 明显大于其它两类焊点。图 4b 小波细节分量极差直方图更加直观地证实了该对应规律。但是该特征信息无法区分另外两类焊点。

图 5 为点焊位移信号标准差与焊点直径的统计分布。统计样本和点焊工艺参数与图 4 相同。图 5a

点焊电极位移信号标准差 D_{STD} 可以将未熔合或未完全熔合焊点与飞溅、合格焊点区分开。部分直径偏小的焊点,在合格临界点附近($\phi 6\text{ mm}$)有部分重叠。这一点在直方图更直观地表示出来,如图 5b 所示。

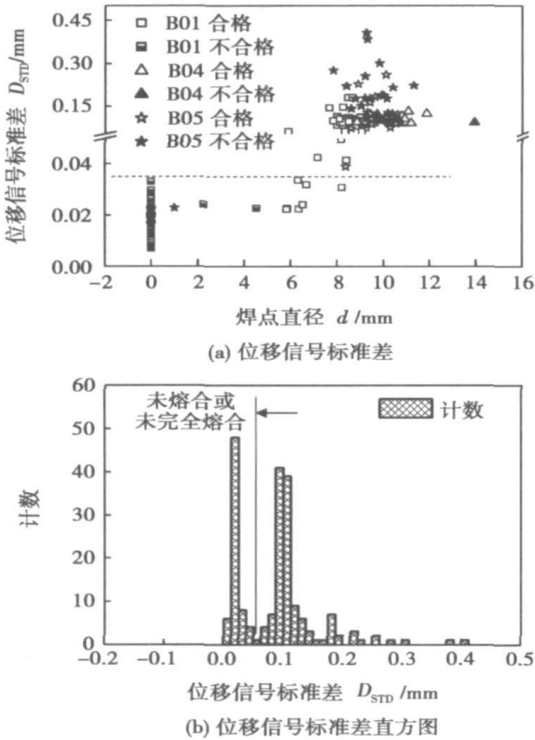


图 5 位移信号标准差与焊点直径的关系
Fig. 5 Relationship between STD of displacement signal and welding spot diameter

图 6 为基于点焊位移信号小波细节分量极差 $D_{DB3/7, \text{range}}$ 和电极位移信号标准差 D_{STD} 的质量判定

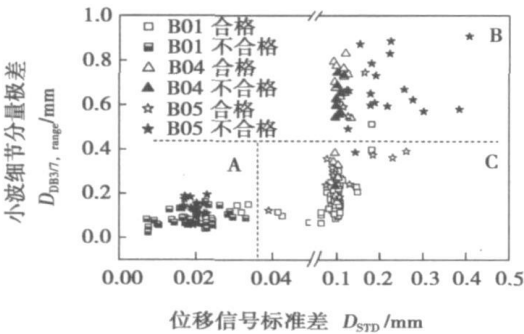


图 6 点焊质量判定与分类
Fig. 6 Resistance spot welding quality judgment and classification

与分类结果。划分三个区域, A 区为未熔合或未完全熔合焊点, B 区为飞溅焊点, C 区为合格焊点。B01 焊点样本 117 个, 分布在 A 区 47 个焊点, 正确判定与分类 85%, 其中, 7 个焊点处于临界区域, 判断错误; 分布在 B 区 3 个焊点, 正确判定与分类 35%; 分布在 C 区 67 个焊点, 正确判定与分类 100%。B04 焊点样本 33 个, 分布在 A 区 0 个焊点, 正确判定与分类 100%; 分布在 B 区 25 个焊点, 正确判定与分类 40%; 分布在 C 区 8 个焊点, 正确判定与分类 88%。B05 焊点样本 47 个, 分布在 A 区 16 个焊点, 正确判定与分类 100%; 分布在 B 区 20 个焊点, 正确判定与分类 85%; 分布在 C 区 11 个焊点, 正确判定与分类 91%。综合上述三种点焊工艺参数, 在合格区焊点 86 个, 只有 2 个判断错误, 正确率高达 97.6%。

4 结 论

采用分布式多传感器同步采集系统实现了铝金点焊质量的实时监测。通过时频域分析发现, 飞溅焊点位移信号在 40 ~ 80 Hz 范围内, Butterworth 带通滤波极差达 0.5 mm; 位移信号极差可以反映未熔合或未完全熔合焊点的质量, 极差也相差 1.0 mm, 质量特征信息明显, 特征提取算法简洁、速度快, 便于实现机器判读。利用统计分析, 样本 197 个焊点, 在合格区内焊点正确判断率高达 97.6%。

参考文献:

[1] 潘存海. 铝合金电阻点焊多传感器信息融合与质量判定[D]. 天津: 天津大学, 2004.
[2] Chien C S, Kannatey-asibu Jr E. Investigation of monitoring systems for resistance spot welding[J]. Welding Journal, 2002, 81(9): 195—199.
[3] 罗贤星, 邓黎鹏, 张晨曙, 等. 铝合金点焊过程中影响因素的特征判识与熔核尺寸的评估[J]. 焊接学报, 2005, 26(7): 37—43.
[4] Burnus C S, Gopinath R A, Guo H T. Introduction to wavelet and wavelet transforms[M]. New Jersey: Prentice-Hall Press, 1998.
[5] 彭玉华. 小波变换与工程应用[M]. 北京: 科学出版社, 2002.

作者简介: 潘存海, 男, 1964 年出生, 博士, 教授。主要从事光机电一体化装备及控制方面的研究工作, 先后参与“863”和主持河北省重大攻关等省部级课题多项, 获省部级科技进步奖 3 项, 发表论文 20 余篇。
Email: pandh@tust.edu.cn

Nanjing University of Technology, Nanjing 210009, China; 2. School of Mechanical and Power Engineering, East China University of Science and Technology, Shanghai 200237, China). p17–20

Abstract The residual stress generated in brazed process and its creep relaxation behavior for stainless steel plate-fin structure at high temperature were analyzed by finite element code ABAQUS. The results show that larger residual stress was generated in brazed joint due to the mismatch mechanical properties between brazing filler metal and base metal and the constraint of clamping fixture. At high temperature region, the residual stress was greatly decreased due to the creep relaxation behavior. The creep stress and strain are concentrated in the fillet zone, where the crack may initiate and propagate along the brazing seam.

Key words: stainless steel plate-fin structure; brazing residual stress; creep relaxation; finite element analysis

Microstructure and wear resistance of laser cladding Co+Ni/WC alloy composite coating YAN Yonggen¹, SI Songhua², ZHANG Hui², HE Yizhu² (1. Baoshan Iron & Steel Co., Ltd, Shanghai 201900, China; 2. School of Material Science and Engineering, Anhui University of Technology, Maanshan 243002, Anhui, China). p21–24

Abstract: Laser cladding Co-based composite coating (Co+Ni/WC) have been obtained on low carbon steel substrate. Microstructure and wear resistance of the composite coatings were investigated compared with the Co-based coating (Co60). It is indicated that the Co60 coating was composed of primary dendrite of γ -Co and the eutectics of γ -Co+Cr₂₃C₆ among the interdendrites, and Co+Ni/WC composite coatings were composed of γ -Co dendrite and the small eutectics which consists of γ -Co, Cr₇C₃, Co₃W₃C and unmelted WC particles. With more WC particles, there was further influence to Co60 coating that the directional solidification of dendrite was changed and the dendrite was finer. Owing to the Ni alloy wrapper, the WC particles had been protected from melt for the diffusion reaction on interface between the WC particles and the Co based alloy. Compared with Co60 coating, the hardness and wear resistance of the Co+Ni/WC composite coatings had been improved and the wear resistance of the Co+20%WC composite coating was twice of that of the Co60 coating.

Key words: laser cladding; Co-based alloy; microstructure; wear resistance

An imaging model for X-ray system and its calibration method TIAN Yuan¹, DU Dong¹, HOU Runshi¹, GAO Zhiling², SHEN Liqun² (1. Department of Mechanical Engineering, Tsinghua University, Beijing 100084, China; 2. Petroleum Steel Pipe Co., Ltd, Qingxian 062650, Hebei, China). p25–28

Abstract: It's one of the most extensive methods to inspect workpiece with X-ray and automatic inspection based on image processing is an important field. The imaging model and calibration establish a geometrical relationship between workpiece and its image, which is the precondition for automatic orientation and measurement with images. Ignored some factors such as the shape of the image in-

tensifier's input screen, the paper develops a model and calibration method for the imaging system used in automatic nondestructive testing system, which is used in weld defect inspection. The results show that the method is effective.

Key words: inspection with X-ray; weld defect; imaging model; calibration

Corrosion of carbon steel joint used modified J422 electrode in ammonium sulfite LEI Ali, ZHANG Shengchao, ZHANG Min (School of Materials Science and Engineering, Xi'an University of Technology, Xi'an 710048, China). p29–32

Abstract Since the welded joint of carbon steel is corroded seriously in the ammonium sulfite, corrosion behavior of welded joint welded by arc welding with J422 electrode containing different contents of Ni has been studied by means of three electrode galvanochemistry test and metallurgical structure analyses. The results show that the addition of Ni causes the grain refinement of the weld and the decrease of acicular ferrite. In addition, the polarizability of the weld increases and the corrosion current decreases in the ammonium sulfite. The welded joint containing 1.2 wt% Ni has the lowest corrosion rate.

Key words: ammonium sulfite; weld decay; alloying; galvanochemistry

Displacement signal time-frequency domain analysis and quality judgment of aluminum alloy resistance spot welding PAN Cunhai¹, DU Sumei¹, SONG Yonglun² (1. School of Mechanical Engineering, Tianjin University of Science and Technology, Tianjin 300222, China; 2. School of Electromechanical Engineering, Beijing University of Technology, Beijing 100085, China). p33–36

Abstract Resistance spot welding quality real-time monitoring of aluminum alloy was realized by distributed multiple-sensor synchronous collection system. Displacement signal time-frequency domain analysis shows that Butterworth band-pass filter range of the expulsion welding spot electrode displacement signal can reach about 0.5 mm between 40–80 Hz. The electrode displacement signal range of the undersize welding spots is lower about 1.0 mm than other two kinds of welding spots, so that using the explicit characteristic information can implement at resistance spot welding quality judgment by man and further can finish quality judgment by machine using the high signal-to-noise displacement signal and the brevity characteristic extracting method. At the same time, statistic analysis of 197 samples indicates that the percentage of accuracy can reach 97.6% at the acceptable welding spots zone.

Key words: resistance spot welding; aluminum alloy; displacement signal; time-frequency domain analysis; quality judgment

Numerical simulation on flow and heat transfer in weld pool of laser-plasma hybrid welding LI Zhining, DU Dong, CHANG Baohua, WANG Li (Key Laboratory for Advanced Materials Processing Technology, Ministry of Education, Tsinghua University, Beijing 100084, China). p37–40

Abstract A unified model is established for the liquid zone,